



## Tin(IV) Halides Zero-dimensional based Inorganic-Organic Hybrid Materials: Crystal Structures and Hirshfeld Surface Analysis

Mamadou Ndiaye<sup>1</sup>, Serigne Fallou Pouye<sup>2,3</sup>, Mouhamadou Birame Diop<sup>2,\*</sup>,  
Libasse Diop<sup>2</sup>, Abdoulaye Samb<sup>1</sup> and Allen G. Oliver<sup>4</sup>

<sup>1</sup>Laboratoire des Produits Naturelles, Département de Chimie, Faculté des Sciences et Techniques, Université Cheikh Anta Diop, Dakar, Sénégal

<sup>2</sup>Laboratoire de Chimie Minérale et Analytique, Département de Chimie, Faculté des Sciences et Techniques, Université Cheikh Anta Diop, Dakar, Sénégal

<sup>3</sup>Département de Sciences Appliquées et Technologies Emergentes, Ecole Supérieure des Sciences et Techniques de l'ingénieur, Université Amadou Mahtar Mbow, Dakar, Sénégal

<sup>4</sup>Department of Chemistry and Biochemistry, University of Notre Dame, Nieuwland, Science Hall, Notre Dame, USA

\*Corresponding author's e-mail: [mouhamadoubdiop@gmail.com](mailto:mouhamadoubdiop@gmail.com)

### Abstract

Two tetramethylguanidinium halostannate inorganic-organic hybrid compounds was isolated and structurally investigated by single crystal X-ray crystallography and Hirshfeld surface analysis. The compound  $[(C_6H_{14}N_3)_2SnCl_6]$  (**1**), crystallizes in the orthorhombic space group *Fddd* with  $Z = 8 / Z' = 0.25$ ,  $a = 7.3474(3) \text{ \AA}$ ,  $b = 22.3678(8) \text{ \AA}$ ,  $c = 28.4908(10) \text{ \AA}$  and  $V = 4682.3(3) \text{ \AA}^3$ . The compound  $[(C_6H_{14}N_3)_2SnBr_6]$  (**2**), crystallizes in the orthorhombic space group *Fddd* with  $Z = 8 / Z' = 0.25$ ,  $a = 7.5767(5) \text{ \AA}$ ,  $b = 23.0591(17) \text{ \AA}$ ,  $c = 29.008(2) \text{ \AA}$  and  $V = 5068.0(6) \text{ \AA}^3$ . The isolation of **1** undergoes a redox process from Sn(II) to Sn(IV) in solution and in a non-controlled atmosphere. Both compounds **1** and **2** describe  $TMG^+$  ions with a central carbon atom in a trigonal-planar fashion. With respect to this  $CN_3$  plane, the pairs of dimethylammonium groups are twisted by  $13.70(8)$  and  $32.21(8)^\circ$  for **1**,  $14.88(13)$  and  $31.95(13)^\circ$  for **2**. The  $SnX_6$  dianions evidence a slightly distorted octahedron (Oh) about Sn centre for hybrids **1** and **2**. Within the structures of the hybrid materials **1** and **2**,  $N-H \cdots Cl$  inter-species

Received: January 16, 2023; Accepted: February 20, 2023; Published: February 22, 2023

Keywords and phrases: single crystal X-ray; tetramethylguanidinium; halostannate; H-bonds; 3D-structure.

Copyright © 2023 the authors. This is an open access article distributed under the Creative Commons Attribution License, which permits unrestricted use, distribution, and reproduction in any medium, provided the original work is properly cited.

hydrogen bonding patterns between the inorganic stannate and the organic entities give rise a one-dimensional chain, wherein inorganic and organic species alternate. The propagation of the chain generates  $R_4^4(12)$  rings. The weak C–H $\cdots$ X hydrogen bonds formed from the methyl groups to adjacent tetramethylguanidinium-stannate chains result in a supramolecular three-dimensional hydrogen-bonded network. The Hirshfeld surface analysis shows existence of both strong and weak hydrogen bonding interactions. Inspection of **1** and **2** by the Hirshfeld surface analysis, show isostructural behavior. Hybrids **1** and **2** are the first crystal reports of a tetramethylguanidinium tetra- or hexahalostannate.

## 1. Introduction

Isolation and designing of inorganic–organic hybrid materials attracted great interest due to the diversity of properties and intriguing topologies they displayed and still arouse [1–8]. In the past, the photodetectors, the semiconductors, the promising applications in solid state cooling systems, the solar cells, absorbers for solar energy conversion, light-emitting device as well as luminescent properties have been found in several inorganic–organic hybrids templated by a diversity of ammonium ions [9–17]. Halostannate hybrid materials constitute a widely studied area, yet either a tetrahalostannate(IV) or hexahalostannate(IV) templated by tetramethylguanidinium has ever been reported. However, the few reports are for polymeric halostannate(II) *viz* guanidinium trichlorostannate(II), [(TMG)SnCl<sub>3</sub>]<sub>n</sub> describing an octahedron arrangement sharing corners [18], diguanidinium tetrachlorostannate(II), [(TMG)<sub>2</sub>SnCl<sub>4</sub>]<sub>n</sub> describing a square pyramid geometry sharing corners [19], tetraguanidinium tetra( $\mu$ -iodo)-tetraiododitin(II), [(TMG)<sub>4</sub>(SnI<sub>4</sub>)<sub>2</sub>]<sub>n</sub> exhibiting an octahedron fashion sharing corners [2], diguanidinium di( $\mu$ -iodo)-diiodo-tin(II), [(TMG)<sub>2</sub>SnI<sub>4</sub>]<sub>n</sub> showing an octahedron sharing corners [2, 3], and tetraiodostannate(II) *ie* diguanidinium tetraiodotin(II), [(TMG)<sub>2</sub>SnI<sub>4</sub>]<sub>n</sub> which evidence an octahedron geometry sharing corners [3]. Indeed, being since a while in focus to widen the inorganic–organic hybrid family compound especially halostannate(IV), the Dakar group has reported crystal structures [20]. In our ongoing of widening this hybrid family of materials, two new hexahalostannate(IV) compounds templated by 1,1,3,3-tetramethylguanidine (TMG), have been isolated. Herein, we report the isolation, the Hirshfeld surface investigation, and the single crystal X-ray diffraction analysis of the two first halostannate(IV) co-crystallizing with TMG<sup>+</sup>, describing inorganic-organic hybrid isostructural 3D-structures, [(TMG)<sub>2</sub>(SnX<sub>6</sub>)]; X = Cl, Br.

## 2. Materials and Methods

### 2.1. General

Reagents were purchased from Sigma-Aldrich, Germany and were used without further purification. Elemental analyses were performed on a Perkin-Elmer model 2400 CHN elemental analyzer. The X-ray crystallographic data for compound **1** and **2** were collected using a Bruker APEX-II DUO diffractometer and a Bruker APEX-II diffractometer, respectively. The Hirshfeld surface analyses were obtained using CrystalExplorer program version 21.5.

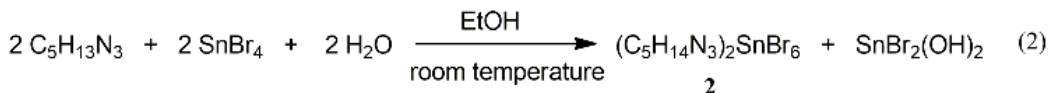
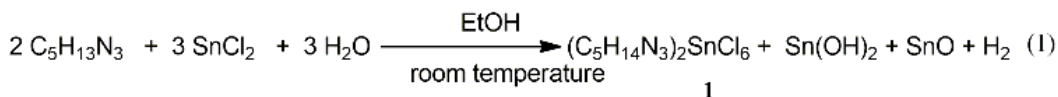
### 2.2. Synthesis of [(TMG)<sub>2</sub>SnCl<sub>6</sub>] (**1**)

In 25 mL ethanolic solution of 1,1,3,3-tetramethylguanidine (TMG), C<sub>5</sub>H<sub>13</sub>N<sub>3</sub> 0.918 g/mL containing 0.6 mL (4.78 mmol) was added dropwise an amount of dichlorotin(II), SnCl<sub>2</sub>·2H<sub>2</sub>O which contained 1.650 g (7.31 mmol) preliminary dissolved in 25 mL of ethanol. The resulting cloudy mixture with gas evolution was stirred at room temperature for about 5h then filtered. After some days of slow evaporation of the filtrate, colorless crystals suitable for single-crystal X-ray diffraction analysis were collected within the supernatant solution and characterized as [(TMG)<sub>2</sub>SnCl<sub>6</sub>] (**1**); yield: 45%. – Anal. calcd. for C<sub>10</sub>H<sub>28</sub>Cl<sub>6</sub>N<sub>6</sub>Sn (563.80 g mol<sup>-1</sup>): C 21.30, H 5.01, N 14.91; found C 21.04, H 5.15, N 14.86.

### 2.3. Synthesis of [(TMG)<sub>2</sub>SnBr<sub>6</sub>] (**2**)

In 25 mL of ethanol, an amount of 1,1,3,3-tetramethylguanidine (TMG), C<sub>5</sub>H<sub>13</sub>N<sub>3</sub> 0.918 g/mL containing 1.3 mL (10.36 mmol) was added. To this ethanolic solution, another amount which contained 4.383 g (10 mmol) of tetrabromotin(IV), SnBr<sub>4</sub> preliminary dissolved in 25mL of ethanol, was added dropwise. The resulting slightly cloudy solution was stirred at room temperature for about 5h then filtered. After a week of slow evaporation of the filtrate, colorless crystals suitable for single-crystal X-ray diffraction analysis were collected within the supernatant solution and characterized as [(TMG)<sub>2</sub>SnBr<sub>6</sub>] (**2**); yield: 60%. – Anal. calcd. for C<sub>10</sub>H<sub>28</sub>Br<sub>6</sub>N<sub>6</sub>Sn (830.50 g mol<sup>-1</sup>): C 14.46, H 3.40, N 10.12; found C 15.00, H 3.35, N 9.98.

The proposed equations of reactions leading to the isolation of compounds **1** and **2** are shown as follows.



## 2.4. X-ray Crystallography

The X-ray crystallographic data of the hybrid **1** was collected using a Bruker APEX-II DUO diffractometer operating at  $T = 100(2)$  K. Data was measured using  $\varphi$  and  $\omega$  scans of  $0.5^\circ$  using  $\text{MoK}\alpha$  radiation ( $\lambda = 0.71073 \text{ \AA}$ ) using a collection strategy to obtain a hemisphere of unique data determined by Apex2 [21]. Cell parameters were determined and refined using the program SAINT [22]. Data was analytically corrected for absorption and polarization effects and analyzed for space group determination, based on measured indexed crystal faces [23]. The structure was solved by dual-space analysis using SHELXT [24] and refined using least-squares minimization with SHELXL [25].

The X-ray crystallographic data of the hybrid **2** was collected using a Bruker APEX-II diffractometer operating at  $T = 120(2)$  K. Data was measured using  $\varphi$  and  $\omega$  scans of  $0.5^\circ$  using  $\text{MoK}\alpha$  radiation ( $\lambda = 0.71073 \text{ \AA}$ ) using a collection strategy to obtain a hemisphere of unique data determined by Apex3 [26]. Cell parameters were determined and refined using the program SAINT [22]. Data was numerically corrected for absorption and polarization effects and analyzed for space group determination [27]. The structure was solved by dual-space analysis using SHELXT [24] and refined using least-squares minimization with SHELXL [25].

Programs used for the representation of the molecular and crystal structures: Olex2 [28] and CrystalExplorer [29]. Crystal data, data collection and structure refinement details for compounds **1** and **2** are summarized in Table 1.

CCDC 2236256 (**1**) and 2236257 (**2**) contain the supplementary crystallographic data for this paper. Copies of these data can be obtained free of charge from the Cambridge Crystallographic Data Centre (CCDC), 12 Union Road, Cambridge CB2 1EZ, UK (fax: int. Code +44 1223 336 033; e-mail: [deposit@ccdc.cam.ac.uk](mailto:deposit@ccdc.cam.ac.uk) or [www: http://www.ccdc.cam.ac.uk](http://www.ccdc.cam.ac.uk)).

**Table 1.** Crystal data and structure refinement of compounds **1** and **2**

Parameters	Compound	
	<b>1</b>	<b>2</b>
Empirical Formula	C <sub>10</sub> H <sub>28</sub> Cl <sub>6</sub> N <sub>6</sub> Sn	C <sub>10</sub> H <sub>28</sub> N <sub>6</sub> Br <sub>6</sub> Sn
Formula weight	563.77	830.53
Temperature (K)	100(2)	120(2)
Crystal system	Orthorhombic	orthorhombic
Space group	Fddd	Fddd
a, (Å)	7.3474(3)	7.5767(5)
α, (°)	90	90
b, (Å)	22.3678(8)	23.0591(17)
β, (°)	90	90
c, (Å)	28.4908(10)	29.008(2)
γ, (°)	90	90
Volume (Å <sup>3</sup> )	4682.3(3)	5068.0(6)
Z/Z'	8/0.25	8/0.25
ρ <sub>calc</sub> (g/cm <sup>3</sup> )	1.599	2.177
μ (mm <sup>-1</sup> )	1.782	10.475
F(000)	2256	3120
Crystal size (mm <sup>3</sup> )	0.194×0.169×0.130	0.285×0.113×0.104
Radiation (Å)	MoKα(λ = 0.71073)	MoKα(λ = 0.71073)
2θ range for data collection (°)	5.72–56.82	4.514–61.236°
	-9 ≤ h ≤ 9	-10 ≤ h ≤ 10
Index ranges	-29 ≤ k ≤ 29	-32 ≤ k ≤ 32
	-38 ≤ l ≤ 36	-41 ≤ l ≤ 41

Parameters	Compound	
	<b>1</b>	<b>2</b>
Reflections collected	32055	52506
Independent reflections	1477 [R <sub>int</sub> = 0.0257]	1966 [R <sub>int</sub> = 0.0442]
Data/restraints/parameters	1477/0/57	1966/0/61
Goodness-of-fit on $F^2$	1.141	1.116
Final R indexes	R <sub>1</sub> = 0.0154	R <sub>1</sub> = 0.0180
[ $I > 2\sigma(I)$ ]	wR <sub>2</sub> = 0.0420	wR <sub>2</sub> = 0.0370
Final R indexes [all data]	R <sub>1</sub> = 0.0160	R <sub>1</sub> = 0.0289
	wR <sub>2</sub> = 0.0428	wR <sub>2</sub> = 0.0397
Largest diff. peak/hole (e Å <sup>-3</sup> )	0.451/-0.600	0.415/-0.481

$R_1 = \Sigma(|F_o| - |F_c|) / \Sigma |F_o|$ ;  $wR_2 = [\Sigma w(F_o^2 - F_c^2)^2 / \Sigma [w(F_o^2)^2]]^{1/2}$  where  $w = 1/[\sigma^2(F_o^2) + 9.2976P + (0.0217P)^2]$  for **1** and  $w = 1/[\sigma^2(F_o^2) + 12.1005P + (0.0154P)^2]$  for **2** where  $P = (F_o^2 + 2F_c^2)/3$ ; ° goodness of fit =  $[\Sigma w(F_o^2 - F_c^2)^2 / (N_o - N_v)]^{1/2}$ .

### 3. Results and Discussion

The inorganic-organic hybrid **1**, [(TMG)<sub>2</sub>SnCl<sub>6</sub>], crystallizes as colorless plate-like crystals in the F-centered, centrosymmetric, orthorhombic space group *Fddd*. The asymmetric unit, is composed of a quarter of the molecule. An ortep view is depicted in Figure 1, comprising one component of the two different species: TMG<sup>+</sup> counter ion, and [SnCl<sub>6</sub>]<sup>2-</sup> complex-anion. The hybrid **2**, [(TMG)<sub>2</sub>SnBr<sub>6</sub>], whose ortep view is represented in Figure 2, crystallizes as colorless block-like crystals in the same F-centered, centrosymmetric, orthorhombic space group *Fddd*.

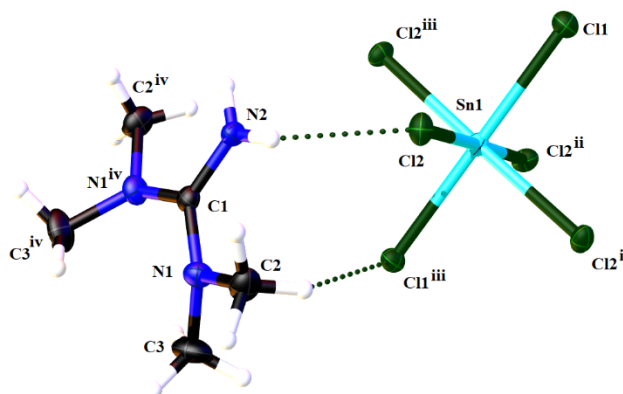


**Figure 1.** Ortep view of **1** showing 50% probability ellipsoids for atoms and the crystallographic numbering scheme [atom color code: H, white; C, black; N, blue; Cl, green; Sn, turquoise] (symmetry codes: (i)  $-x+5/4, y, -z+5/4$ ; (ii)  $-x+5/4, -y+5/4, z$ ; (iii)  $x, -y+5/4, -z+5/4$ ; (iv)  $-x+1/4, -y+5/4, z$ ).

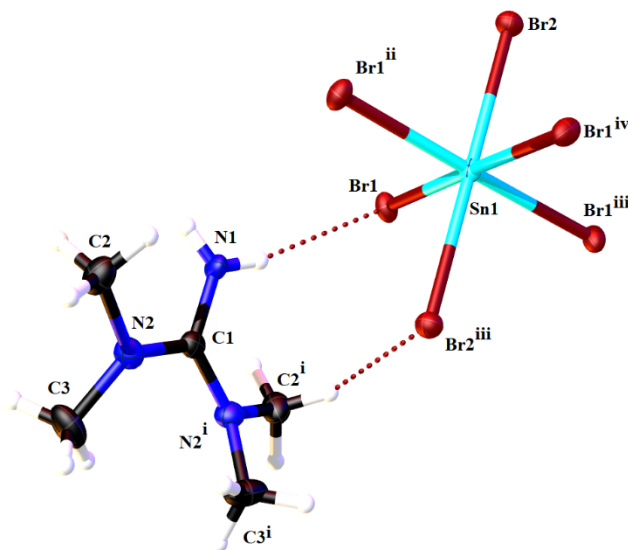


**Figure 2.** Ortep view of **2** showing 50% probability ellipsoids for atoms and the crystallographic numbering scheme [atom color code: H, white; C, black; N, blue; Br, red; Sn, turquoise] (symmetry codes: (i)  $x, -y+3/4, -z+3/4$ ; (ii)  $-x+7/4, -y+3/4, z$ ; (iii)  $-x+7/4, y, -z+3/4$ ; (iv)  $-x+3/4, -y+3/4, z$ ).

The isolation of **1** results from a redox process over the dichlorotin(II) dihydrate,  $\text{SnCl}_2 \cdot 2\text{H}_2\text{O}$  used as starting material, when the reaction is carried out in ethanolic solution and in a non-controlled atmosphere. Indeed, the Sn(II) has been oxidized to form Sn(IV). For **1**, the C–N length, C–N–C and N–C–N angle values (see Table 2) within the  $\text{TMG}^+$  ions are in accordance with the reported values for this cation, describing a central atom C1 in an almost trigonal–planar configuration [30–32]. Moreover, the C–N bond length values of 1.325(2) and 1.3435(14) Å indicate a partial double-bond character. Thus, its positive charge may be considered to be delocalized in the  $\text{CN}_3$  plane. The two pairs of dimethylammonium groups are twisted by 13.70(8) and 32.21(8)° with respect to the  $\text{CN}_3$  plane. In comparison to **1**, compound **2** also exhibits a central atom C1 in an almost trigonal–planar configuration, the three N–C–N angles ranging from 119.6(2) to 120.19(12)° (Table 2). The corresponding C–N bond length values of 1.318(3) and 1.340(2) Å indicate a partial double-bond character too. Hence, once more the positive charge can be considered to be delocalized in the  $\text{CN}_3$  plane. In addition, the two pairs of dimethylammonium groups, compared to those in **1**, are twisted by 14.88(13) and 31.95(13)° with respect to the  $\text{CN}_3$  plane. The geometric parameters within the  $\text{SnX}_6$  dianions (Table 2) well corroborate, as earlier encountered in the literature [5, 8, 20, 33–35], a slightly distorted octahedron (Oh) about Sn centre for hybrids **1** and **2**. Primarily, structures of compound **1** and **2** can be count as discrete wherein the inorganic hexa-halostannate complex-anion is connected to two organic  $\text{TMG}^+$  counter cations.

In the structures of the hybrid materials **1** and **2**, each inorganic specie is surrounded by four organic species (Figures 3 and 4). In the contrary to the six bonded halotin(IV) inorganic component, each organic specie is surrounded by two inorganic ones [Figures 5(a) and 6(a)].

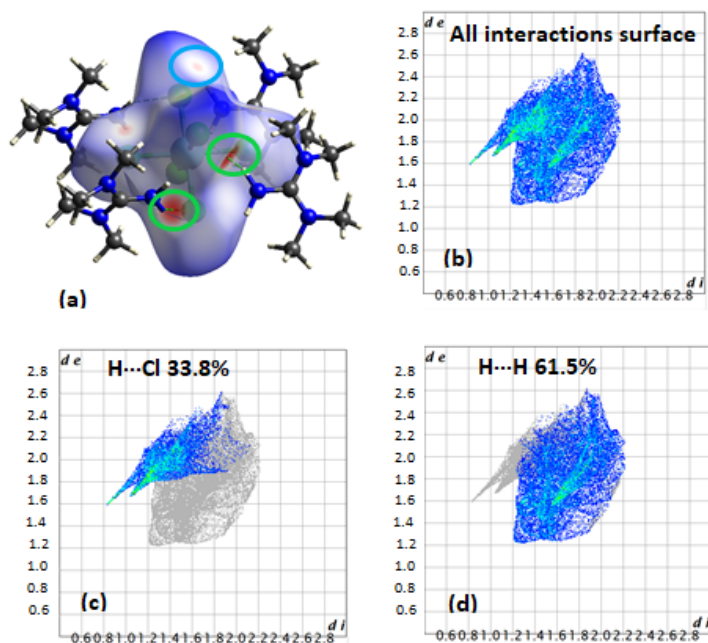


**Figure 3.** View of  $[\text{SnCl}_6]^{2-}$  complex-anion to be surrounded with a  $d_{\text{norm}}$  decorated Hirshfeld Surface and the cations surrounding it in ball and stick presentations for compound **1** (a). The red areas in the green and cyan ellipses indicate  $\text{H}\cdots\text{Cl}$  contact points ( $\text{N}-\text{H}\cdots\text{Cl}$  and  $\text{C}-\text{H}\cdots\text{Cl}$ , respectively). The outline of the full fingerprint contribution (b), most important type of interactions  $\text{H}\cdots\text{Cl}$  (c), and  $\text{H}\cdots\text{H}$  (d) interactions in the fingerprint plot diagram.

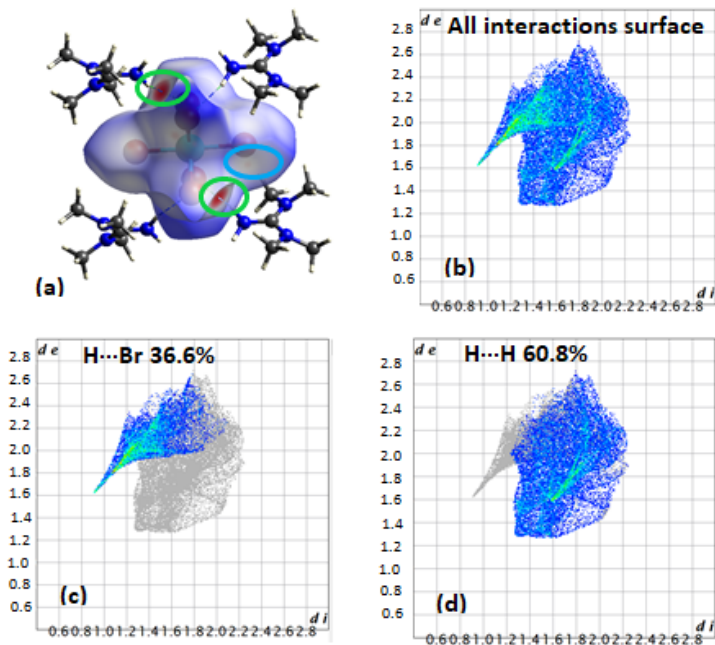


**Figure 4.** View of [SnBr<sub>6</sub>]<sup>2-</sup> complex-anion to be surrounded with a  $d_{\text{norm}}$  decorated Hirshfeld Surface and the cations surrounding it in ball and stick presentations for compound **2** (a). The red areas in the green and cyan ellipses indicate H...Br contact points (N-H...Br and C-H...Br, respectively). The outline of the full fingerprint contribution (b), most important type of interactions H...Br (c), and H...H (d) interactions in the fingerprint plot diagram.

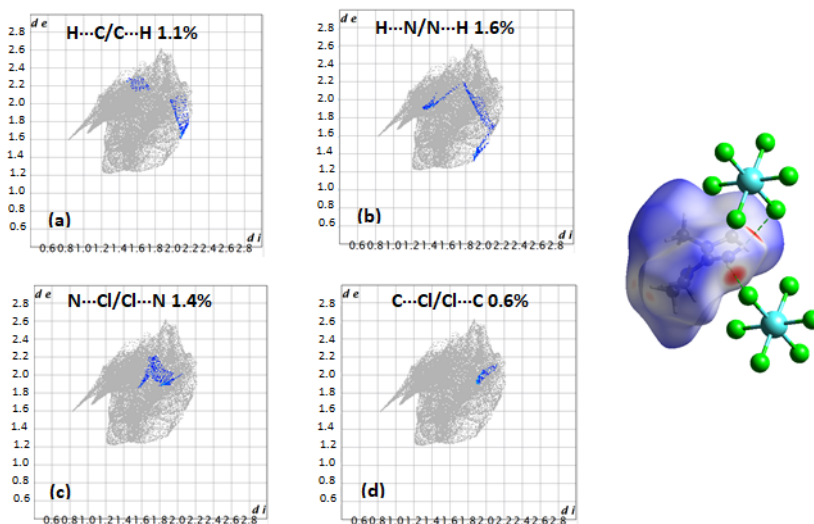


**Figure 5.** View of the cation  $[\text{TMG}]^+$  presented with a  $d_{\text{norm}}$  decorated Hirshfeld Surface and the anions surrounding it in ball and stick (right). Contribution of the trace interactions (a)  $\text{H}\cdots\text{C}/\text{C}\cdots\text{H}$ , (b)  $\text{H}\cdots\text{N}/\text{N}\cdots\text{H}$ , (c)  $\text{N}\cdots\text{Cl}/\text{Cl}\cdots\text{N}$ , and (d)  $\text{C}\cdots\text{Cl}/\text{Cl}\cdots\text{C}$  derived from the fingerprint plot of compound **1**.

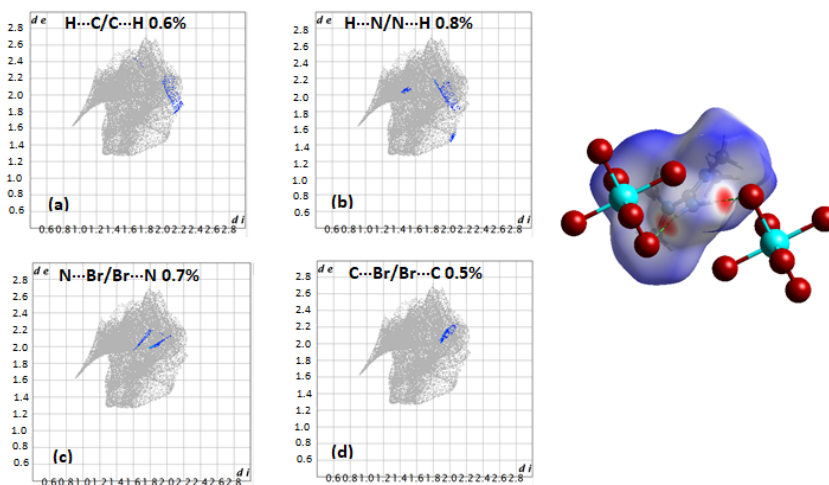


**Figure 6.** View of the cation  $[\text{TMG}]^+$  presented with a  $d_{\text{norm}}$  decorated Hirshfeld Surface and the anions surrounding it in ball and stick (right). Contribution of the trace interactions (a)  $\text{H}\cdots\text{C}/\text{C}\cdots\text{H}$ , (b)  $\text{H}\cdots\text{N}/\text{N}\cdots\text{H}$ , (c)  $\text{N}\cdots\text{Br}/\text{Br}\cdots\text{N}$ , and (d)  $\text{C}\cdots\text{Br}/\text{Br}\cdots\text{C}$  derived from the fingerprint plot of compound **2**.

**Table 2.** Selected prominent geometric parameters (Å,°) for compounds **1** and **2** [Symmetry codes for **1**: (i)  $-x+5/4, y, -z+5/4$ ; (ii)  $-x+5/4, -y+5/4, z$ ; (iii)  $x, -y+5/4, -z+5/4$ ; (iv)  $-x+1/4, -y+5/4, z$ ; Symmetry codes for **2**: (i)  $x, -y+3/4, -z+3/4$ ; (ii)  $-x+7/4, -y+3/4, z$ ; (iii)  $-x+7/4, y, -z+3/4$ ; (iv)  $-x+3/4, -y+3/4, z$ ].

<b>1</b>		<b>2</b>	
Atom-Atom	Bond length	Atom-Atom	Bond length
Sn1–Cl2	2.4371 (3)	Sn1–Br1	Sn1–Br1
Sn1–Cl2 <sup>i</sup>	2.4371 (3)	Sn1–Br1 <sup>i</sup>	Sn1–Br1 <sup>i</sup>
Sn1–Cl2 <sup>ii</sup>	2.4371 (3)	Sn1–Br1 <sup>ii</sup>	Sn1–Br1 <sup>ii</sup>
Sn1–Cl2 <sup>iii</sup>	2.4371 (3)	Sn1–Br1 <sup>iii</sup>	Sn1–Br1 <sup>iii</sup>
Sn1–Cl1	2.4327 (4)	Sn1–Br2 <sup>iii</sup>	Sn1–Br2 <sup>iii</sup>
Sn1–Cl1 <sup>iii</sup>	2.4327 (4)	Sn1–Br2	Sn1–Br2
N1–C1	1.3435 (14)	N2–C1	1.340 (2)
N1–C2	1.4630 (17)	N2–C2	1.458 (3)
N1–C3	1.4641 (18)	N2–C3	1.464 (3)
N2–C1	1.325 (2)	N1–C1	1.318 (3)
<b>1</b>		<b>2</b>	
Atom-Atom-Atom	Angle value	Atom-Atom-Atom	Angle value
Cl2–Sn1–Cl2 <sup>iii</sup>	90.249 (15)	Br1–Sn1–Br1 <sup>ii</sup>	178.731 (8)
Cl2–Sn1–Cl2 <sup>i</sup>	89.760 (15)	Br1 <sup>ii</sup> –Sn1–Br1 <sup>iii</sup>	90.156 (10)
Cl2 <sup>iii</sup> –Sn1–Cl2 <sup>ii</sup>	89.760 (15)	Br1–Sn1–Br1 <sup>iii</sup>	89.859 (9)
Cl2 <sup>iii</sup> –Sn1–Cl2 <sup>i</sup>	178.946 (14)	Br1–Sn1–Br1 <sup>i</sup>	90.155 (10)
Cl2–Sn1–Cl2 <sup>ii</sup>	178.946 (14)	Br1 <sup>ii</sup> –Sn1–Br1 <sup>i</sup>	89.858 (10)
Cl2 <sup>ii</sup> –Sn1–Cl2 <sup>i</sup>	90.250 (15)	Br1 <sup>i</sup> –Sn1–Br1 <sup>iii</sup>	178.732 (8)
Cl1–Sn1–Cl2	90.526 (7)	Br1 <sup>iii</sup> –Sn1–Br2	89.366 (4)
Cl1–Sn1–Cl2 <sup>i</sup>	89.472 (7)	Br1 <sup>ii</sup> –Sn1–Br2	90.634 (4)

Cl1 <sup>iii</sup> –Sn1–Cl2 <sup>ii</sup>	89.472 (7)	Br1–Sn1–Br2	90.635 (4)
Cl1 <sup>iii</sup> –Sn1–Cl2 <sup>iii</sup>	90.526 (7)	Br1 <sup>i</sup> –Sn1–Br2 <sup>iii</sup>	90.634 (4)
Cl1 <sup>iii</sup> –Sn1–Cl2	89.474 (7)	Br1 <sup>i</sup> –Sn1–Br2	89.366 (4)
Cl1–Sn1–Cl2 <sup>iii</sup>	89.474 (7)	Br1 <sup>iii</sup> –Sn1–Br2 <sup>iii</sup>	90.634 (4)
Cl1 <sup>iii</sup> –Sn1–Cl2 <sup>i</sup>	90.528 (7)	Br1–Sn1–Br2 <sup>iii</sup>	89.365 (4)
Cl1–Sn1–Cl2 <sup>ii</sup>	90.528 (7)	Br1 <sup>ii</sup> –Sn1–Br2 <sup>iii</sup>	89.366 (4)
Cl1 <sup>iii</sup> –Sn1–Cl1	180.0	Br2 <sup>iii</sup> –Sn1–Br2	180.0
C1–N1–C2	120.29 (12)	C1–N2–C2	120.73 (18)
C1–N1–C3	121.13 (12)	C1–N2–C3	120.92 (18)
C2–N1–C3	114.93 (12)	C2–N2–C3	115.28 (18)
N2–C1–N1 <sup>iv</sup>	120.18 (8)	N1–C1–N2	120.19 (12)
N2–C1–N1	120.18 (8)	N1–C1–N2 <sup>iv</sup>	120.19 (12)
N1–C1–N1 <sup>iv</sup>	119.63 (17)	N2 <sup>iv</sup> –C1–N2	119.6 (2)

In the crystal of **1** and **2**, the N–H···Cl inter-species hydrogen bonding interactions between the inorganic stannate and the organic ones, enable the extension into a one-dimensional chain of hydrogen-bonded moieties parallel to the crystallographic 100 direction, wherein (TMG)<sub>2</sub>SnX<sub>6</sub> represents the repeating pattern with alternating inorganic/organic species (see Figures 7 and 8). The propagation of the chain describes  $R_4^4(12)$  rings (see Figures 7 and 8, and Tables 3 and 4).

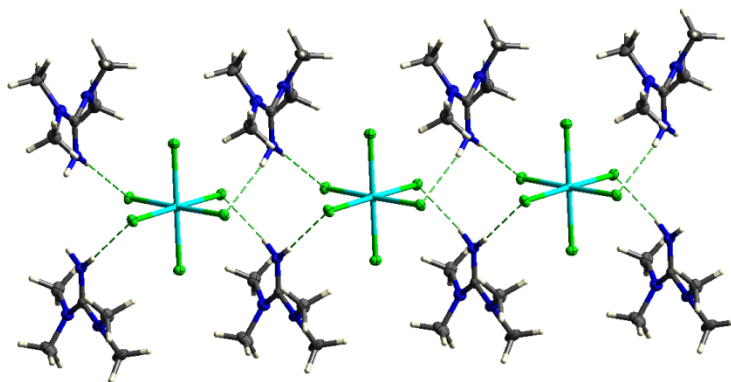


**Figure 7.** View of **1** showing the  $R_4^4(12)$  macrocyclic ring enabling the growth of the hydrogen bonded chain parallel to the [100] direction.

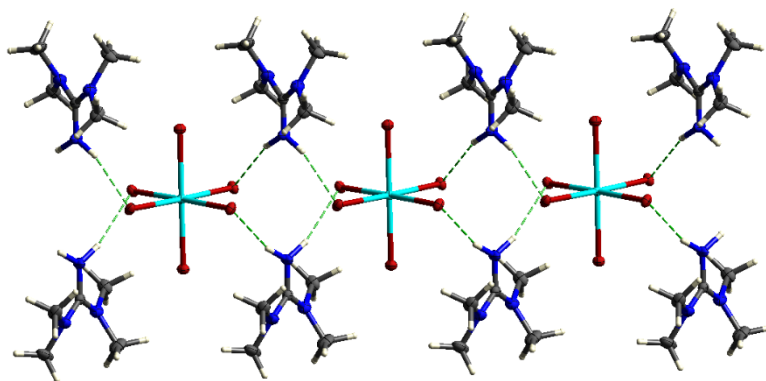


**Figure 8.** View of **2** showing the  $R_4^4(12)$  macrocyclic ring enabling the growth of the hydrogen bonded chain parallel to the  $[100]$  direction.

**Table 3.** Hydrogen-bonds geometry in the crystal of **1** [Symmetry codes: (iii)  $x, -y+5/4, -z+5/4$ ; (iv)  $-x+1/4, -y+5/4, z$ ; (v)  $-x+1, y-1/4, z-1/4$ ; (vi)  $x-1/4, -y+1, z-1/4$ ].

D–H $\cdots$ A	$d(D-H)$	$d(H\cdots A)$	$d(D\cdots A)$	$\angle(D-H\cdots A)$
N2–H2A $\cdots$ C12	0.88	2.56	3.3741(10)	155
N2–H2B $\cdots$ C12 <sup>iv</sup>	0.88	2.56	3.3741(10)	155
C2–H2C $\cdots$ C11 <sup>iii</sup>	0.98	3.03	3.7887(15)	135
C2–H2D $\cdots$ C11 <sup>v</sup>	0.98	2.82	3.6581(14)	144
C3–H3B $\cdots$ C12 <sup>vi</sup>	0.98	2.85	3.7350(16)	151

**Table 4.** Hydrogen-bonds geometry in the crystal of **2** [Symmetry codes: (iv)  $-x+3/4, -y+3/4, z$ ; (v)  $x-3/4, -y+1, z+1/4$ ; (vi)  $-x+3/4, y, -z+3/4$ ; (vii)  $-x+1, y+1/4, z+1/4$ ].

D–H $\cdots$ A	$d(D-H)$	$d(H\cdots A)$	$d(D\cdots A)$	$\angle(D-H\cdots A)$
N1–H1N $\cdots$ Br1 <sup>iv</sup>	0.80(2)	2.75(2)	3.5279(16)	167
C2–H2B $\cdots$ Br2 <sup>v</sup>	0.98	2.98	3.774(2)	139
C2–H2C $\cdots$ Br2 <sup>vi</sup>	0.98	3.10	3.861(2)	136
C3–H3C $\cdots$ Br1 <sup>vii</sup>	0.98	2.96	3.821(2)	147

It is noteworthy to outline the presence of weaker C–H $\cdots$ X hydrogen bonding patterns from the methyl groups to adjacent tetramethylguanidinium-stannate chains resulting in a supramolecular three-dimensional hydrogen-bonded framework (see Figure 9, Tables 3 and 4). Additional interactions (C3–H3A $\cdots$ N1  $d(D\cdots A) = 2.8787(19)$  Å  $\angle(D-H\cdots A) = 103^\circ$  and C3–H3A $\cdots$ N2  $d(D\cdots A) = 2.866(3)$  Å  $\angle(D-H\cdots A) = 102^\circ$ ) involving one methyl group, are as well present. These interactions enable the structure to grow stronger in compactness and stability. In the structure of the inorganic-organic hybrid **1**, the separation between Sn centres within chains Sn1 $\cdots$ Sn1 =  $a = 7.3474(3)$  Å while that between the closest Sn centres of adjacent chains Sn1 $\cdots$ Sn1 =  $9.2400(2)$  Å. In comparison to the structure of **1**, the hybrid **2** describes Sn1 $\cdots$ Sn1 =  $a = 7.5767(5)$  Å separation between Sn centres within chains and Sn1 $\cdots$ Sn1 =  $9.4558(5)$  Å separation between the closest Sn centres of adjacent chains, which compare well.

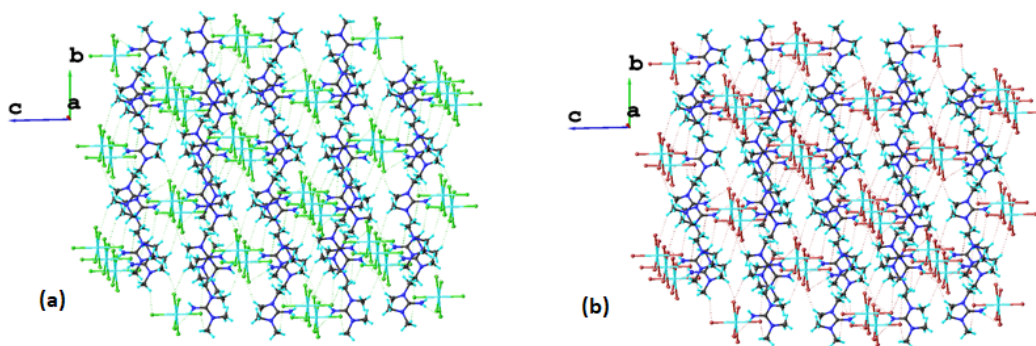


**Figure 9.** View of hybrid **1** (a) and **2** (b) showing the resulting hydrogen bonded 3D structure.

Crystals of the hybrids **1** and **2** have been investigated by Hirshfeld surface analysis using CrystalExplorer 21.5 [29]. The Hirshfeld surface analysis corroborate the existence of both strong and weak hydrogen bonding patterns (Figures 3(a) and 4(a)). The most prominent contacts are shown to be H $\cdots$ X and H $\cdots$ H (Figures 3(c), (d) and 4(c), (d)).

Finally, close inspection of the two hybrids **1** and **2**, show that they are isostructural. The isostructural fashion for these hexa-halostannate hybrids is evidences by the Hirshfeld surface analysis with the similarities observed by closely inspecting the shape index and curvedness plots of **1** and **2** (Figure 10).

To the best of our knowledge, there are no previously reported structures of a

tetramethylguanidinium tetra- or hexa-halostannate. However, the closest species are reports of guanidinium hexa-fluorostannate and hexa-chlorostannate [13, 36, 37].

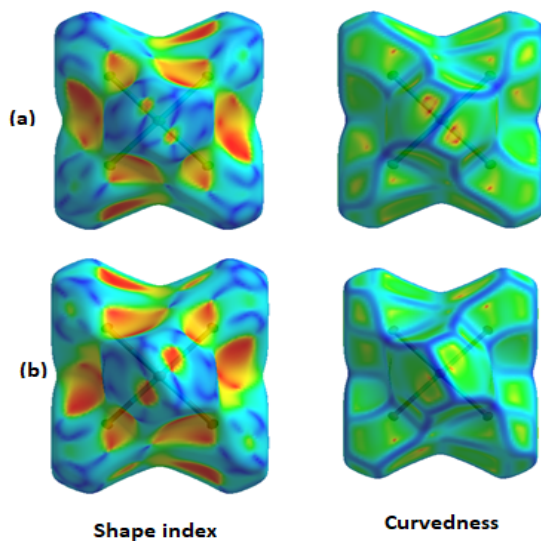


**Figure 10.** Shape Index and curvedness of compounds **1(a)** and **2(b)**.

#### 4. Conclusion

The reaction between tetramethylguanidine and, dichlorotin(II) dihydrate or tetrabromotin(IV) led to the isolation of two new hexa-halostannate based inorganic-organic hybrid complexes which have been investigated by single crystal X-ray diffraction and Hirshfeld surface analyses. Both hybrids **1** and **2** describe a hexa-halostannate anion in a distorted octahedral geometry, hydrogen bonded to tetramethylguanidinium cations affording 1D infinite chains connected, through weaker hydrogen bonding interactions, in a supramolecular three dimensional-like structure. To our knowledge, such a self-assembly organization between hexa-halostannate and tetramethylguanidinium antagonistic ions has ever been encountered. Thus, the isostructural structures of hybrids **1** and **2** evidence the first examples of tetramethylguanidinium hexa-halostannate inorganic-organic hybrid. In our ongoing attempts to isolate and characterize new halostannate based hybrids templated by various dissymmetric amines, further works are in progress.

#### Conflicts of Interest

There are no conflicts to declare.

## Acknowledgement

The authors gratefully acknowledge the Cheikh Anta Diop University (Senegal), the University of Notre Dame (USA) and Dr. Khalil Abboud (University of Florida, USA) for equipment facilities.

## References

- [1] Zhang, L., Luo, Z., Wang, W., Liu, Y., He, X., & Quan, Z. (2022). Organic cation-directed modulation of emissions in zero-dimensional hybrid tin bromides. *Inorganic Chemistry*, 61(37), 14857-14863. <https://doi.org/10.1021/acs.inorgchem.2c02438>
- [2] Daub, M., Haber, C., & Hillebrecht, H. (2017). Synthesis, crystal structures, optical properties, and phase transitions of the layered guanidinium-based hybrid perovskites  $[C(NH_2)_3]_2MI_4$ ;  $M = Sn, Pb$ . *European Journal of Inorganic Chemistry*, 2017(7), 1120-1126. <https://doi.org/10.1002/ejic.201601499>
- [3] Stoumpos, C.C., Mao, L., Malliakas, C.D., & Kanatzidis, M.G. (2017). Structure–band gap relationships in hexagonal polytypes and low-dimensional structures of hybrid tin iodide perovskites. *Inorganic Chemistry*, 56(1), 56-73. <https://doi.org/10.1021/acs.inorgchem.6b02764>
- [4] Zhou, C., Lin, H., Shi, H., Tian, Y., Pak, C., Shatruk, M., Zhou, Y., Djurovich, P., Du, M. H., & Ma, B. (2018). A zero-dimensional organic seesaw-shaped tin bromide with highly efficient strongly stokes-shifted deep-red emission. *Angewandte Chemie International Edition*, 57(4), 1021-1024. <https://doi.org/10.1002/anie.201710383>
- [5] Zhou, C., Tian, Y., Wang, M., Rose, A., Besara, T., Doyle Nicholas, K., Yuan, Z., Wang Jamie, C., Clark, R., Hu, Y., Siegrist, T., Lin, S., & Ma, B. (2017). Low-dimensional organic tin bromide perovskites and their photoinduced structural transformation. *Angewandte Chemie International Edition*, 56(31), 9018-9022. <https://doi.org/10.1002/anie.201702825>
- [6] Herrmann, H., Walter, P., Kaifer, E., & Himmel, H.J. (2017). Incorporation of a redox-active bis(guanidine) in low-dimensional tin and lead iodide structures. *European Journal of Inorganic Chemistry*, 2017(47), 5539-5544. <https://doi.org/10.1002/ejic.201700840>
- [7] Kaiba, A., Al Otaibi, F., Geesi, M.H., Riadi, Y., Aljohani, T.A., & Guionneau, P. (2021) A new organic–inorganic hybrid compound  $(NH_3(CH_2)C_6H_4CO_2H)[SnCl_6]$ : Synthesis, crystal structure, vibrational, optical, magnetic properties and theoretical study. *Journal of Molecular Structure*, 1234, 130129. <https://doi.org/10.1016/j.molstruc.2021.130129>

- [8] Su, B., Song, G., Molokeev, M.S., Lin, Z., & Xia, Z. (2020). Synthesis, crystal structure and green luminescence in zero-dimensional tin halide  $(C_8H_{14}N_2)_2SnBr_6$ . *Inorganic Chemistry*, 59(14), 9962-9968. <https://doi.org/10.1021/acs.inorgchem.0c01103>
- [9] Nazarenko, O., Kotyrba, M.R., Yakunin, S., Wörle, M., Benin, B.M., Rainò, G., Krumeich, F., Kepenekian, M., Even, J., Katan, C., & Kovalenko, M.V. (2019). Guanidinium and mixed cesium-guanidinium tin(II) bromides: Effects of quantum confinement and out-of-plane octahedral tilting. *Chemistry of Materials*, 31(6), 2121-2129. <https://doi.org/10.1021/acs.chemmater.9b00038>
- [10] Zhou, C., Lin, H., Tian, Y., Yuan, Z., Clark, R., Chen, B., van de Burgt, L. J., Wang, J. C., Zhou, Y., Hanson, K., Meisner, Q. J., Neu, J., Besara, T., Siegrist, T., Lambers, E., Djurovich, P., & Ma, B. (2018). Luminescent zero-dimensional organic metal halide hybrids with near-unity quantum efficiency. *Chemical Science*, 9(3), 586-593. <https://doi.org/10.1039/c7sc04539e>
- [11] Zhu, H. L., Liang, Z., Huo, Z., Ng, W. K., Mao, J., Wong, K. S., Yin, W.-J. & Choy, W. C. H. (2018). Low-bandgap methylammonium-rubidium cation Sn-rich perovskites for efficient ultraviolet–visible–near infrared photodetectors. *Advanced Functional Materials*, 28 (16), 1706068. <https://doi.org/10.1002/adfm.201706068>
- [12] Zhou, C., Tian, Y., Yuan, Z., Lin, H., Chen, B., Clark, R., Dilbeck, T., Zhou, Y., Hurley, J., Neu, J., Besara, T., Siegrist, T., Djurovich, P., & Ma, B. (2017). Highly efficient broadband yellow phosphor based on zero-dimensional tin mixed-halide perovskite. *ACS Applied Materials & Interfaces*, 9(51), 44579-44583. <https://doi.org/10.1021/acsami.7b12862>
- [13] Szafranski, M., & Stahl, K. (2016). Phase transitions in layered diguanidinium hexachlorostannate(IV). *Crystal Growth & Design*, 16(4), 2157-2166. <https://doi.org/10.1021/acs.cgd.5b01830>
- [14] Noel, N.K., Stranks, S.D., Abate, A., Wehrenfennig, C., Guarnera, S., Haghghirad, A.-A., Sadhanala, A., Eperon, G.E., Pathak, S.K., Johnston, M.B., Petrozza, A., Herz, L.M., & Snaith, H.J. (2014). Lead-free organic-inorganic tin halide perovskites for photovoltaic applications. *Energy & Environmental Science*, 7(9), 3061-3068. <https://doi.org/10.1039/C4EE01076K>
- [15] Hao, F., Stoumpos, C.C., Guo, P., Zhou, N., Marks, T.J., Chang, R.P.H., & Kanatzidis, M.G. (2015). Solvent-mediated crystallization of  $CH_3NH_3SnI_3$  films for heterojunction depleted perovskite solar cells. *Journal of the American Chemical Society*, 137(35), 11445-11452. <https://doi.org/10.1021/jacs.5b06658>

- [16] Giorgi, G., Fujisawa, J.-I., Segawa, H., & Yamashita, K. (2015). Organic–inorganic hybrid lead iodide perovskite featuring zero dipole moment guanidinium cations: A theoretical analysis. *Journal of Physical Chemistry C*, 119(9), 4694-4701. <https://doi.org/10.1021/acs.jpcc.5b00051>
- [17] Dimesso, L., Quintilla, A., Kim, Y.-M., Lemmer, U., & Jaegermann, W. (2016). Investigation of formamidinium and guanidinium lead tri-iodide powders as precursors for solar cells. *Materials Science and Engineering B*, 204, 27-33. <https://doi.org/10.1016/j.mseb.2015.11.006>
- [18] Szafranski, M., & Stahl, K. (2007). Crystal structure and phase transitions in perovskite-like  $C(NH_2)_3SnCl_3$ . *Journal of Solid State Chemistry*, 180(8), 2209-2215. <https://doi.org/10.1016/j.jssc.2007.05.024>
- [19] Szafranski, M., & Stahl, K. (2000). Pressure-induced decoupling of the order-disorder and displacive contributions to the phase transition in diguanidinium tetrachlorostannate. *Physical Review B*, 62(13), 8787-8793. <https://doi.org/10.1103/PhysRevB.62.8787>
- [20] Diop, M.B., Sarr, M., Cissé, S., Diop, L., Oliver, A.G., & Akkurt, M. (2020). A “Zero-Dimensional Hybrid” tin(IV) chloride from a Sn-C bond cleavage: Synthesis, infrared and X-ray single-crystal molecular characterization. *International Journal of Engineering Research and Applications*, 10(10), 17-23. <https://doi.org/10.9790/9622-1010031723>
- [21] Apex2, Crystallographic Software, Suite, Bruker AXS Inc., Madison, Wisconsin, USA, 2014.
- [22] SAINT (Version 8.34A), Area Detector Integration Software, Bruker AXS Inc., Madison, Wisconsin, USA, 2012.
- [23] Bruker AXS Inc., Madison, Wisconsin, USA, 2014.
- [24] Sheldrick, G.M. (2015). *SHELXT* - Integrated space-group and crystal structure determination. *Acta Crystallographica*, A71(1), 3-8. <https://doi.org/10.1107/S2053273314026370>
- [25] Sheldrick, G.M. (2015). Crystal structure refinement with SHELXL. *Acta Crystallographica*, C71(1), 3-8. <https://doi.org/10.1107/S2053229614024218>
- [26] Apex3, Crystallographic Software, Suite, Bruker AXS, Madison, Wisconsin, USA, 2016.
- [27] Krause, L., Herbst-Irmer, R., Sheldrick, G.M., & Stalke, D. (2015). Comparison of silver and molybdenum microfocus X-ray sources for single-crystal structure determination. *Journal of Applied Crystallography*, 48, 3-10. <https://doi.org/10.1107/S1600576714022985>

- [28] Dolomanov, O.V., Bourhis, L.J., Gildea, R.J., Howard, J.A.K., & Puschmann, H. (2009). OLEX2: a complete structure solution, refinement and analysis program. *Journal of Applied Crystallography*, 42(2), 339-341. <https://doi.org/10.1107/S0021889808042726>
- [29] Spackman, P.R., Turner, M.J., McKinnon, J.J., Wolff, S.K., Grimwood, D.J., Jayatilaka, D., & Spackman, M.A. (2021). CrystalExplorer: a program for Hirshfeld surface analysis, visualization and quantitative analysis of molecular crystals. *Journal of Applied Crystallography*, 54(3), 1006-1011. <https://doi.org/10.1107/S1600576721002910>
- [30] Giltzau, N.O., & Köckerling, M. (2018). Bis(tetramethylguanidinium) hexachloridotellurate(IV). *IUCrData*, 3(10), x181488. <https://doi.org/10.1107/S2414314618014888>
- [31] Ndiaye, M., Samb, A., Diop, L., & Maris, T. (2016). Crystal structure of catena-poly[N,N,N',N'-tetramethylguanidinium [(chloridocadmate)-di- $\mu$ -chlorido]]. *Acta Crystallographica*, E72(1), 1-3. <https://doi.org/10.1107/S2056989015020836>
- [32] Ndiaye, M., Samb, A., Diop, L., & Maris, T. (2016). Crystal structure of bis-(N,N,N',N'-tetramethylguanidinium) tetrachloridocuprate(II). *Acta Crystallographica*, E72(7), 1047-1049. <https://doi.org/10.1107/S2056989016010161>
- [33] Rgaieg, R., Karoui, K., & Zouari, R. (2017). Synthesis, crystal structure and electrical properties of (C<sub>3</sub>H<sub>13</sub>NCl)<sub>2</sub>SnCl<sub>6</sub>. *Phase Transitions*, 90(10), 1034-1048. <https://doi.org/10.1080/01411594.2017.1302086>
- [34] Zhou, L., Zhang, L., Li, H., Shen, W., Li, M., & He, R. (2021). Defect passivation in air-stable tin(IV)-halide single crystal for emissive self-trapped excitons. *Advanced Functional Materials*, 31(51), 2108561. <https://doi.org/10.1002/adfm.202108561>
- [35] Liu, Y., Li, Y.-K., Ying, T.-T., Tan, Y.-H., Tang, Y.-Z., Han, D.-C., Du, P.-K., & Zhang, H. (2021). Multisequential reversible phase transition materials with semiconducting and fluorescence properties: (C<sub>3</sub>H<sub>18</sub>BrN)<sub>2</sub>SnBr<sub>6</sub>. *New Journal of Chemistry*, 45(44), 20721-20725. <https://doi.org/10.1039/D1NJ04448F>
- [36] Ishida, H., Furukawa, Y., & Kashino, S. (1999). Bis(guanidinium) hexachlorostannate(IV). *Acta Crystallographica*, C55(12), 1995-1997. <https://doi.org/10.1107/S0108270199012032>
- [37] Calov, U., Schneider, M., & Leibnitz, P. (1991). Guanidiniumhexafluorometallate von Titan, Silicium, Germanium und Zinn. Guanidiniumpentafluorooxonioibat und Guanidiniumtetrafluorodioxowolfram. *Zeitschrift für anorganische und allgemeine Chemie*, 604(1), 77-83. <https://doi.org/10.1002/zaac.19916040111>